UC Davis
UC Davis Previously Published Works

Title

Absence of backscattering in Fermi-arc mediated conductivity of the topological Dirac semimetal Cd3As2

Permalink

https://escholarship.org/uc/item/58h150k8

Journal

Physical Review B, 109(19)

ISSN

Authors

Ivanov, Vsevolod

Borkowski, Lotte

Wan, Xiangang

et al.

Publication Date

2024-05-01

DOI

Copyright Information

Peer reviewed

culations [1, 4, 23, 30, 44], which are inherently limited by the large number of atoms in its crystal unit cell. In particular, this makes first-principles investigations of the surface state physics of Cd_3As_2 especially difficult on account of the even larger supercells involved.

The Dirac points in Cd_3As_2 can be considered as composed of opposite chirality Weyl points, which are connected by Fermi arcs at the material surface [41]. It has been shown that the Fermi arcs in Weyl semimetals can be highly conductive [31], prompting the question of whether the Fermi arc states of Dirac semimetals can lead to similar transport effects. This question is particularly relevant for the case of cadmium arsenide, which has been shown to exhibit extraordinarily high electronic transport even in thin-film and nanowire geometries [20, 24, 36, 42, 53], where surface effects would be expected to dominate.

Here we perform a numerical study of the electronic transport of Cd_3As_2 mediated by its Fermi arc surface states. We begin by empirically deriving a tight–binding model fit to the first-principles electronic structure, and use it to construct a 40-layer slab supercell to extract the surface energy bands. We show that contrast to prior $k \cdot p$ models [44], the Fermi arcs of Cd_3As_2 in our *ab initio*-based model are long and straight, extending across the entire BZ to connect across the zone boundary. By performing explicit calculations of the phase space available to electronic scattering we demonstrate that two major scattering contributions become vanishingly small regardless of the scattering mechansim. This can po-

I. INTRODUCTION.

Cadmium arsenide (Cd_3As_2) is a well known semiconductor that has been thoroughly studied for the greater part of a century for its remarkable transport properties [40]. More recently, this material was predicted [44] and confirmed using angle-resolved photoemission spectroscopy [5, 26, 33, 48] to be a topological Dirac semimetal . A conventional Dirac semimetal exists at the boundary between topological insulator (TI) and normal insulator phases in a system possessing both time-reversal and inversion symmetries, and hosts a Dirac node at a time-reversal invariant momentum point in the Brillouin zone (BZ) [47]. However, such a phase can also exist when the crystal structure possesses a rotational axis [11], such as the C_4 rotation in Cd_3As_2, which can result in accidental band crossings at the Fermi energy, leading to two topologically protected Dirac points along the $\Gamma - Z$ direction [44].

The properties of cadmium arsenide have been well established through a number of experimental works, in which it served as a prototypical system for demonstrating the optical conductivity [6, 14, 25], quantum oscillations [21, 49, 53], electronic transport [3, 19, 20, 22, 36, 39, 52] of Dirac semimetal materials. Dirac semimetals were additionally predicted to exhibit proximity-induced superconductivity [16], and Cd_3As_2 was used in experimental realizations of this effect [12, 18, 37, 43].

Cadmium arsenide also received limited theoretical treatment using models [27, 44] and first-principles cal-

tentially lead to very high conductance in thin films of Cd_3As_2. We further extend this argument in the presence of an external electric field, where we show that the induced symmetry–breaking results in a weak topological insulator phase, whose surface states preserve the essential properties necessary for high electronic mobility. We conclude by discussing how these results might lead to next-generation electronic devices based on the high electronic mobility of the surface states and their potential hydrodynamic transport, and how such long, straight Fermi arcs might be engineered in semiconductor heterostructures.

II. MATERIAL BACKGROUND.

Although research on the properties of Cd_3As_2 has been reinvigorated by the confirmation of its topological electronic structure [5], the material itself has been known to exist for nearly a century [40]. At high temperatures, cadmium arsenide adopts a ten–atom anti–fluorite structure ($Fm\bar{3}m$ #225) with two cadmium vacancies [40]. Upon cooling to $\sim 600°C$, the remaining cadmium atoms displace towards the ordered vacancies, resulting in a the intermediate structure with a distorted $\sqrt{2} \times \sqrt{2} \times 2$ supercell ($P4_2/nmc$ #137) of the original cubic structure [29]. Below $\sim 475°C$, the material settles into its low–temperature phase, which is a $2 \times 2 \times 4$ superstructure of the ten–atom anti-fluorite cell. The exact nature of this low temperature phase has been somewhat controversial, initially being assigned to the inversion-broken $I4_1cd$ (#110) space group [38], which was recently reexamined and found to actually be the centrosymmetric $I4_1acd$ (#142) [1]. This has important consequences for the electronic structure, preserving the Dirac crossings in the BZ, and enabling the possibility of tuning the topological phase by breaking inversion symmetry.

The topological nature of the electronic structure in Cd_3As_2 has been confirmed experimentally with transport and angle-resolved photoemission spectroscopy (ARPES) measurements.

Electronic excitations around the Dirac cones at the Fermi level of Cd_3As_2 behave like relativistic Dirac fermions with linear dispersion. These excitations have extremely large Fermi velocities [36], and are expected to lead to large electronic mobilities which have been observed experimentally [19, 20, 36]. Surprisingly, these high electron mobilities persist even in thin–films and nanowires of Cd_3As_2 [24, 27, 36, 42]. Bulk-boundary correspondence in topological materials [9] implies that topological features in the bulk exist in tandem with topologically protected surface states, which in the case of bulk Dirac points take the form of Fermi arcs connecting their projections on the surface. Such Fermi arcs are known to be highly conductive for related Weyl semimetal systems [31], and would be expected to dominate the transport properties of Cd_3As_2 in thin–film and nanowire geometries.
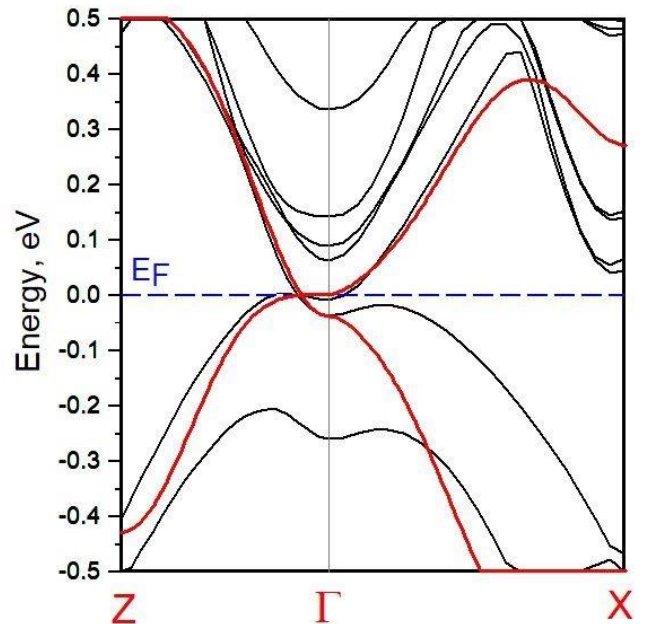

FIG. 1. Electronic structure of Cd_3As_2 derived from first principles density functional based calculation(black), and its tight binding fit (red).

ARPES measurements enable the direct observation of bulk and surface states. This has allowed the linearly dispersing Dirac cones at the Fermi surface to be directly observed [5, 26, 33, 48]. The derived $\boldsymbol{k} \cdot \boldsymbol{p}$ model [44] predicts the existence of short Fermi arcs enclosing the Γ point, and later studies of the Weyl–semimetal state in symmetry–broken Cd_3As_2 using a model derived from Wannier interpolation also predict short arcs [30]. However, the $\boldsymbol{k} \cdot \boldsymbol{p}$ model necessarily represents only the behavior near the Γ-point, poorly capturing the electronic structure at the BZ edge, and experimental ARPES measurements have yet to observe Fermi arc surface states. It has been suggested that the difficulty in observing Fermi arc surface states in Dirac semimetals might stem from their lack of topological protection [15], and in fact there exist Dirac systems that completely lack Fermi arcs [17].

Directly simulating these surface states from first principles would be computationally prohibitive, as such a calculation would require a slab supercell consisting of at least several dozen enormous unit cells of Cd_3As_2. The inclusion of spin-orbit coupling in order to correctly capture the topological electronic structure, and the dense $\boldsymbol{k}$-point grids needed to obtain the Fermi surface would further complicate this approach. On the other hand, a $\boldsymbol{k} \cdot \boldsymbol{p}$ model, while quick to compute, would not be able accurately represent the electronic structure throughout the entire BZ. The most optimal approach, which admits a trade–off of speed and accuracy, is a tight-binding model.
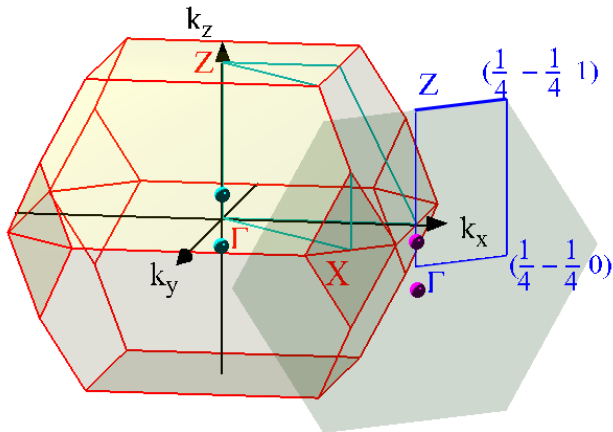
3

by very long, straight Fermi arcs (Fig. 3b). In contrast to $k \cdot p$ calculations [44], these arcs do not enclose the Γ point, and instead extend through the entire BZ to connect across the BZ boundary. The origin of the arcs can be understood in terms of the $\pm$ chirality Weyl points comprising each Dirac point. Each pair of Weyl points located at opposite momentum space k-points are connected by a single Fermi arc. The two Dirac points of Cd_3As_2 can be thought of as two pairs of coincident Weyl points of anti-aligned chiralities, with each pair having its own Fermi arc. An important feature of the Fermi arcs is the spin-texture; spins along each arc point along opposite directions, but rotate as they approach the Dirac node projections to align with local "all-out" arrangement around each point.

FIG. 2. The Brillouin Zone (BZ) of bulk Cd_3As_2 and its projection along the $langle110\rangle$ direction that is used for calculating the surface states. The blue rectangle shows the portion of the surface BZ that will be used in subsequent plots. The bulk Dirac points along $\Gamma - Z$ and their projections onto the surface BZ are indicated by small circles.

III. ELECTRONIC STRUCTURE OF Cd_3As_2

We perform self-consistent density functional–based electronic structure calculation of Cd_3As_2 using the full potential linear muffin–tin orbital method (FPLMTO) including spin–orbit coupling [34]. The band structure plotted along the $Z - \Gamma - X$ direction shown in Fig. 1, clearly reveals the four-fold degenerate Dirac point along the $\Gamma - Z$ direction which is protected by the C_4 rotational symmetry of the crystal [11], and is consistent with previous studies of Cd_3As_2 [1].

In order to numerically study the topological surface states of Cd_3As_2 and their transport properties, we derive a tight–binding model by empirically fitting the electronic structure. Our model captures the essence of the electronic behavior throughout the (BZ), and accurately reproduces the four-fold topological Dirac point along the $\Gamma - Z$ direction as shown in red in Fig. 1. (We describe the tight-binding fit and list the parameters of the model in the Supplemental Material)

Using this tight–binding model we construct a 40-layer slab in the $\langle110\rangle$ direction, by first extending the model over the supercell and then forbidding hoppings between the top and bottom surfaces. The relationship between Brillouin Zones for the bulk and the slab is shown in Fig. 2.

The resulting band structure can be plotted within the plane spanned by the $k_{\langle1-10\rangle} = k_{xy}$ and $k_{\langle001\rangle} = k_z$ vectors, shown in Figure 3a). The surface states arising from the topological Dirac nodes are clearly visible as the only states crossing the Fermi energy.

Plotting the Fermi surface of the slab calculation reveals that the two Dirac point projections are connected
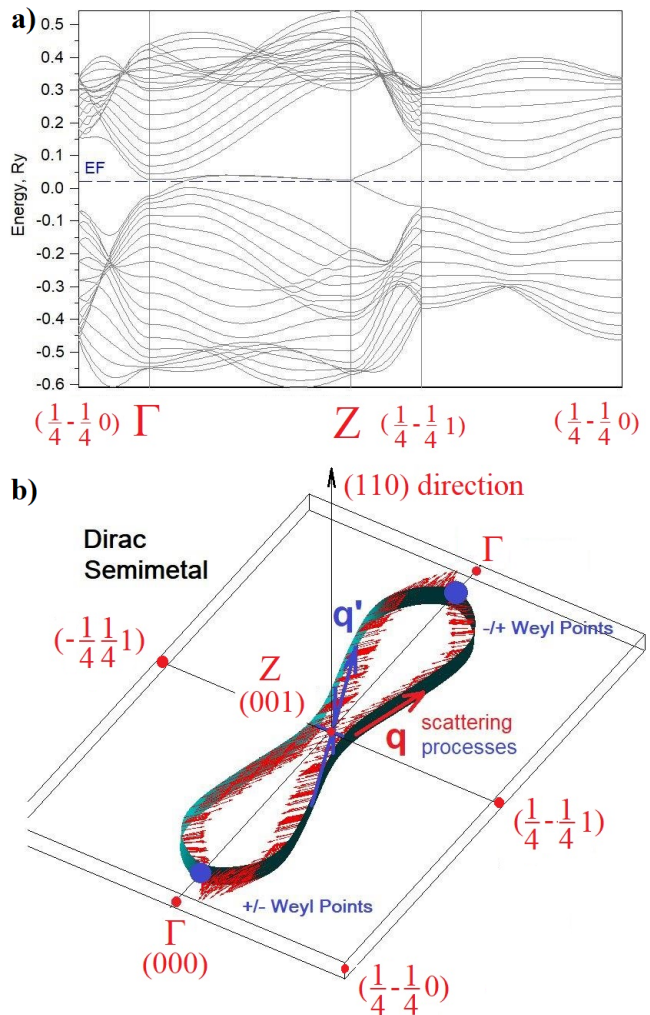

FIG. 3. 40-layer slab calculation of the tight-binding model fit for the Dirac semimetal phase of Cd_3As_2, showing the a) band structure, and b) Fermi arc surface states. Note that the shown region is stretched along the $k_{\langle1-10\rangle}$ direction in order to more clearly show the arc shape.

IV. TRANSPORT ANALYSIS

We now proceed to the analysis of the surface–mediated transport in Cd_3As_2 from first principles. The relaxation rate of the electrons due to impurities or phonons is related to the matrix element of their scattering potential. This usually results in a temperature–independent impurity contribution to the resistivity of a metal often seen at very low temperatures, with an electron–phonon contribution that scales linearly with temperature, $\rho_{e-ph}(T) \propto \lambda_{tr}T$, where λ_{tr} is the so called transport coupling constant, which captures the scattering processes of the electrons near the Fermi surface. It can be obtained from an integral over the Brillouin Zone $\lambda_{tr} = \sum_{\boldsymbol{q}} = \lambda_{tr}(\boldsymbol{q})$ [2], of various scattering events subjected to the momentum and energy conservation laws:

$$\lambda_{tr}(\boldsymbol{q}) \sim \sum_{\boldsymbol{k}} (v_{\boldsymbol{k}\alpha} - v_{\boldsymbol{k}+\boldsymbol{q}\alpha})^2 |V_{\boldsymbol{k}\boldsymbol{k}+\boldsymbol{q}}|^2 \delta(\epsilon_{\boldsymbol{k}})\delta(\epsilon_{\boldsymbol{k}+\boldsymbol{q}}). \quad (1)$$

Here, $\epsilon_{\boldsymbol{k}}$, $\epsilon_{\boldsymbol{k}+\boldsymbol{q}}$ are the energies and $v_{\boldsymbol{k}\alpha}$, $v_{\boldsymbol{k}+\boldsymbol{q}\alpha}$ are the Fermi velocities at points $\boldsymbol{k}, \boldsymbol{k} + \boldsymbol{q}$ in the phase space. The delta functions $\delta(\epsilon_{\boldsymbol{k}})$, $\delta(\epsilon_{\boldsymbol{k}+\boldsymbol{q}})$ constrain scattering to the Fermi surface. The transport direction is set by $\alpha = x, y, z$, while $V_{\boldsymbol{k}\boldsymbol{k}+\boldsymbol{q}}$ is the matrix element of the potential arising from either impurities or atomic displacements induced by a phonon with wavevector $\boldsymbol{q}$. For the spinor states of the electrons, it has both spin and spatial contributions which can be accounted for in a factored form for non–magnetic impurities or phonons: $V_{\boldsymbol{k}\boldsymbol{k}+\boldsymbol{q}} = V_{\boldsymbol{k}\boldsymbol{k}+\boldsymbol{q}}^{spin} V_{\boldsymbol{k}\boldsymbol{k}+\boldsymbol{q}}^{space}$.

Generally, electron–phonon resistivity calculations can be carried out for real materials from completely first principles [31, 35]. The same is true for supercell simulations with impurities, however, the large unit cell of Cd_3As_2 expanded to a 40-layer slab contains thousands of atoms and would make such direct approaches computationally intractable. Instead, we use our previously derived tight-binding fit to perform the analysis of the phase space available to scattering using Eq.(1), and derive our conclusions based on this phase space calculation.

For a slab extended in the $\langle 110 \rangle$ direction, the BZ will be highly compressed along $k_{\langle 110 \rangle}$, therefore we use a two-dimensional 800×800 $\boldsymbol{k}$-point grid for the integration in Eq.(1). Since the Fermi arcs are very narrow along the $k_{\langle 1-10 \rangle}$ direction, the $\boldsymbol{q}$-point region for visualizing $\lambda_{tr}(\boldsymbol{q})$ is selected to be a part of the BZ, spanned by the corners $(1/4, -1/4, 0)$, $(-1/4, 1/4, 0)$ in the $(2\pi/a, 2\pi/a, 2\pi/c)$ units of the reciprocal space.

Before discussing the numerical results, we qualitatively consider the behavior of the phase space available to scattering. The main contributions to $\lambda_{tr}(\boldsymbol{q})$ are known to be the back–scattering processes since in this case the electronic velocities entering Eq.(1) will point in opposite directions. The back–scattering ($\boldsymbol{k} \to -\boldsymbol{k}$) occurs in every three dimensional Fermi surface but would be absent for a true Weyl semimetal since its Fermi arcs reside on different surfaces. However, this is no longer

true in a Dirac semimetal where both Fermi arcs appear at the same surface. We however, notice here that aside from small regions near the Dirac point projections, the spinor states on opposite Fermi arcs are anti-aligned as seen in Fig. 3b. This makes such back–scattering processes strongly cancel each other for non magnetic impurities or phonons, due to the orthogonality of spinors with opposite spins. In contrast, side-scattering ($\boldsymbol{k} \to \boldsymbol{k'}$) can occur between any two momentum points along each Fermi arc. The magnitude of this contribution depends on the Fermi velocity term $(v_{\boldsymbol{k}\alpha} - v_{\boldsymbol{k}+\boldsymbol{q}\alpha})^2$, where the velocities are oriented perpendicular to the arc. For the long, straight Fermi arcs that we find in Cd_3As_2, electrons are only scattered between states with parallel velocities, thus reducing this contribution to zero. This is analogous to the case of Fermi arc states in Weyl semimetals such as TaAs [31] and NbAs [50].

These contributions can be visualized (Figure 4) in the $\boldsymbol{q}$-dependence of the phase space integral by adding each term in the expression (1) iteratively. First, we evaluate the bare contribution $\sum_{\boldsymbol{k}} \delta(\epsilon_{\boldsymbol{k}})\delta(\epsilon_{\boldsymbol{k}+\boldsymbol{q}})$, shown in Figure 4(a). The effect of the dumbbell-like structure of the Fermi arcs is apparent here, forming two bright bands flanking a bowtie-shape along the central strip of the $\boldsymbol{q}$-space. While this term lacks the velocity pre–factor of the full expression and cannot be quantitatively compared to the other calculations, it clearly shows all of the allowed transitions within the phase space.

Next we add the velocity contribution, computing the integral $\sum_{\boldsymbol{k}} (v_{\boldsymbol{k}\alpha} - v_{\boldsymbol{k}+\boldsymbol{q}\alpha})^2 \delta(\epsilon_{\boldsymbol{k}})\delta(\epsilon_{\boldsymbol{k}+\boldsymbol{q}})$, shown in Fig. 4(b). This greatly reduces the amplitude of side scattering processes along the Fermi arcs extended in the q_z direction, evidenced by the disappearance of the central bowtie structure in the phase space.

We can also quantitatively compare the effect of including the spin term $\sum_{\boldsymbol{k}} (v_{\boldsymbol{k}\alpha} - v_{\boldsymbol{k}+\boldsymbol{q}\alpha})^2 |V_{\boldsymbol{k}\boldsymbol{k}+\boldsymbol{q}}^{spin}|^2 \delta(\epsilon_{\boldsymbol{k}})\delta(\epsilon_{\boldsymbol{k}+\boldsymbol{q}})$, since for non–magnetic scatterering processes this reduces to evaluating the overlap between two spinor states of the electrons. The result is shown in 4(c), where we also indicate the scales of the obtained phase space functions since the integrals with and without $|V_{\boldsymbol{k}\boldsymbol{k}+\boldsymbol{q}}^{spin}|^2$ have the same units. As one can see, the effect of including the spinor overlaps results in the complete suppression of the back–scattering terms, making their contributions to λ_{tr} almost negligible throughout the entire phase space, as evidenced in Fig. 4(c) and its comparison with 4(b) (note the difference in scales). The only remaining contributions are faint regions at the edge, which correspond to weak scattering terms between $\boldsymbol{k}$-points located near opposite Dirac node projections.

The results obtained here can naturally explain recent low temperature resistivity measurements of Cd_3As_2 [19], where it was found that some samples below 5K exhibited very long transport lifetimes, up to 10^4 longer than the quantum lifetimes. The resistivity anisotropy was observed to be 20–30 in samples with large lifetime enhancements, along with measured ultrahigh carrier mobilities
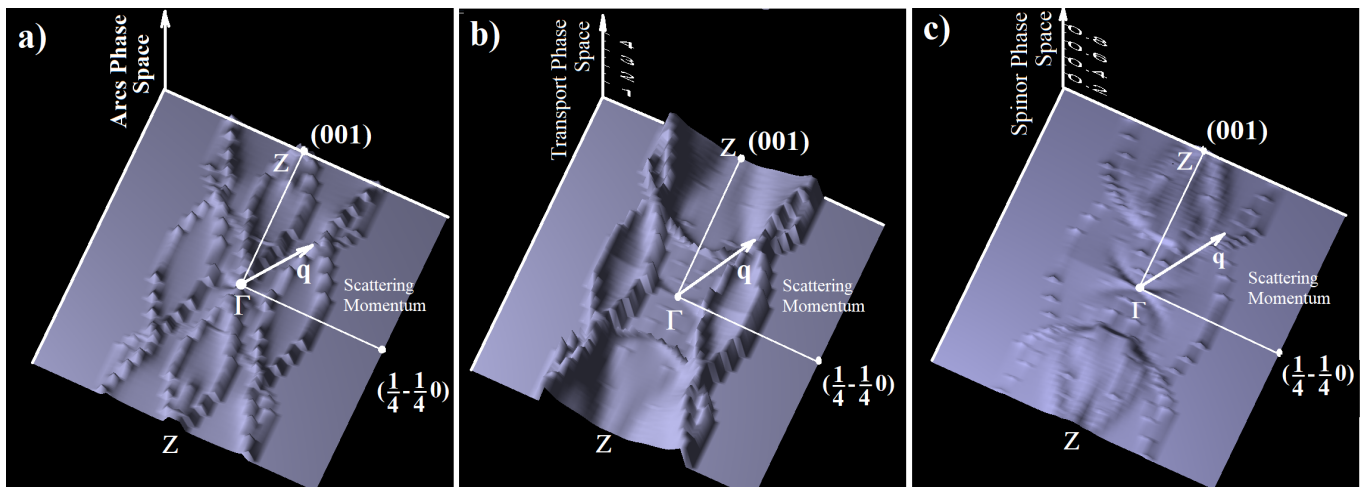
FIG. 4. Phase space calculation of scattering processes involving Fermi arc electrons in Cd_3As_2. Case (a) is the double-delta integral, (b) includes the velocity prefactor and (c) includes both velocity and spin prefactors. Note that the normalization factor in (a) differs from the other two plots so only (b) and (c) can be compared quantitatively.

that were claimed to be protected by an "unknown mechanism" [19]. Although such a behavior would indeed be unexpected for bulk Dirac cone states in Cd_3As_2, it is easily understood if the surface transport at very low temperatures is taken into account. Here, in the absence of thermally activated carriers at the bulk, the Fermi arc surface states would be the main contributor to the conductivity, so strong anistoropy and very large carrier mobility are expected as seen from our phase space calculation with the strongly suppressed back– and side–scattering events.

V. TOPOLOGICAL INSULATOR PHASE

We now proceed to the analysis of the Cd_3As_2 surface states in the presence of an inversion breaking term. This can occur either in the vicinity of the contact interface with the electrical leads or when a strong electric field is applied. Both effects can naturally occur along the $\langle 110 \rangle$ growth direction, breaking the inversion and C_4 rotation symmetries of the system, and introducing a small gap at the Dirac points. This symmetry–breaking effect can be modeled at the level of the crystal structure by introducing small opposite shifts of the Cd cations and As anions along the $\langle 110 \rangle$ direction. It can be easily analyzed based on a $4 \times 4 \boldsymbol{k} \cdot \boldsymbol{p}$ model Hamiltonian. (See Supplemental Material for details)

Gapping a Dirac point along a high symmetry line can result in either a Weyl semimetal or topological insulator (TI) [47]. We eliminate the first possibility by employing the monopole mining method [13], which finds no sources/sinks of Berry curvature within the BZ. For the second case, we determine the classification [8, 9] of the TI phase by explicitly computing the topological indices on each torus using a discretized plaquette link method [7, 10]. This identifies a weak TI phase, which is confirmed by our calculation of (a) the surface energy band

states (Figure 5a) with the Dirac cone appearing around zone boundary Z point of the Brillouin Zone, and of the Fermi surface sheets crossing the edges of the BZ (Figure 5b) instead of encircling the Γ point as they would for a strong TI.

The Fermi surface of the Cd_3As_2 TI phase is qualitatively very similar to the Dirac semimetal phase. Fermi surface sheets have long straight regions extended in the $\Gamma - Z$ direction, as well as the anti–aligned spin structure at $(\mathbf{k}, -\mathbf{k})$ opposite $\mathbf{k}$-points. The only deviations from this are slight spin rotations near the Γ point, where the Dirac node projections were previously located. Overall however, this Fermi surface structure would similarly suppress both back and side-scattering processes, resulting in a highly suppressed scattering just as in the Dirac phase.

VI. CONCLUSION

In conclusion, based on our accurate numerical fits to the electronic structure of Dirac semimetal Cd_3As_2, we have computed the surface states in a slab geometry, finding Fermi arcs that stretch through the edges of the Brillouin Zone and produce very long and straight Fermi surfaces. Their particular shape and spin structure results in suppression of both back– and side– scattering effects in the electronic transport, which was explicitly demonstrated by calculating the available phase space to the scattering for the Fermi arc electrons of the Dirac semimetal phase. A similar suppression mechanism is expected for the surface states of a possible weak topological insulator phase, that can be induced by an inversion–breaking perturbation. Ultra–high carrier mobility and strong resistivity anisotropy at very low temperatures naturally emerges from the present study which could explain recent resistivity measurements in Cd_3As_2 [19].
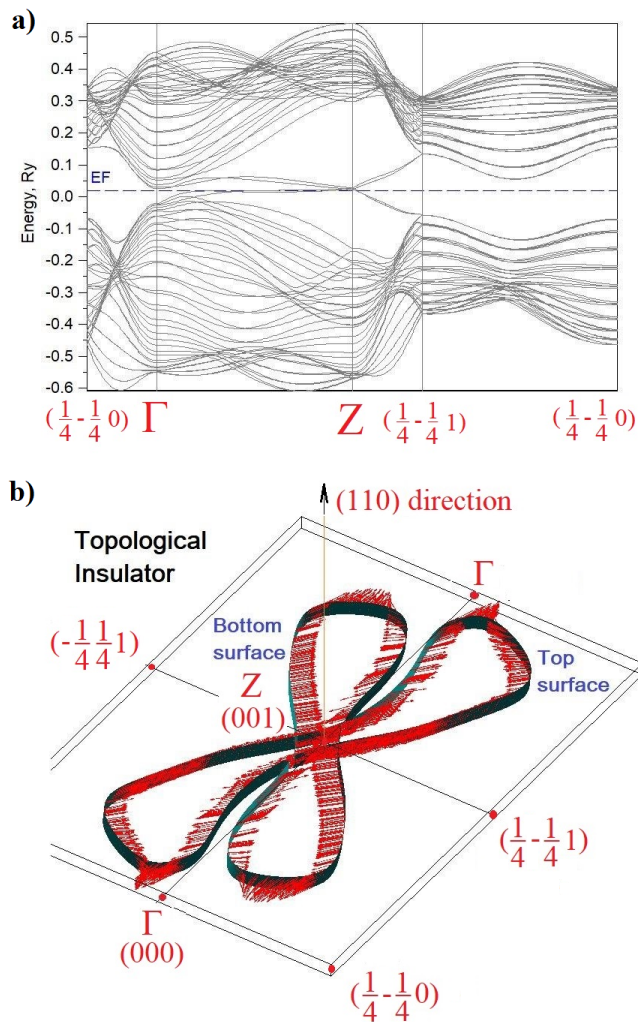
Recently, a number of approaches have emerged for engineering topological Dirac states in semiconductor heterostructures [28, 45, 51]. The mature fabrication methods developed around these Group-III, -IV, and -V semiconductors enable the creation of heterostructures with precise control over layer thickness, termination, doping, and strain. Since the shape of Fermi arc surface states is highly dependent on the crystallographic direction of the surface, the atomic terminations, surface strain, and material interfaces [32, 46], these highly–tunable semiconductor heterostructures could be used to engineer long, straight, Fermi arc states with high mobilities for next–generation electronic devices.

ACKNOWLEDGMENTS

FIG. 5. 40-layer slab calculation of the tight-binding model fit for the topological insulator phase of Cd_3As_2, showing the a) band structure, and b) surface states. Note that the shown region is stretched along the $k_{\langle 1-10 \rangle}$ direction in order to more clearly show the surface states.

[1] Mazhar N. Ali, Quinn Gibson, Sangjun Jeon, Brian B. Zhou, Ali Yazdani, and R. J. Cava. The crystal and electronic structures of cd3as2, the three-dimensional electronic analogue of graphene. *Inorganic Chemistry*, 53(8):4062–4067, 2014. PMID: 24679042.

[2] P. B. Allen. New method for solving boltzmann's equation for electrons in metals. *Phys. Rev. B*, 17:3725–3734, May 1978.

[3] Yuriko Baba, Francisco Domínguez-Adame, Gloria Platero, and Rafael A Molina. Rashba coupling and spin switching through surface states of dirac semimetals. *New Journal of Physics*, 23(2):023008, feb 2021.

[4] Santu Baidya and David Vanderbilt. First-principles theory of the dirac semimetal cd3as2 under zeeman magnetic field. *Phys. Rev. B*, 102:165115, Oct 2020.

[5] Sergey Borisenko, Quinn Gibson, Danil Evtushinsky, Volodymyr Zabolotnyy, Bernd Büchner, and Robert J.

Cava. Experimental realization of a three-dimensional dirac semimetal. *Phys. Rev. Lett.*, 113:027603, Jul 2014.

[6] Guoqing Chang, Jia-Xin Yin, Titus Neupert, Daniel S. Sanchez, Ilya Belopolski, Songtian S. Zhang, Tyler A. Cochran, Zǐji ā Chéng, Ming-Chien Hsu, Shin-Ming Huang, Biao Lian, Su-Yang Xu, Hsin Lin, and M. Zahid Hasan. Unconventional photocurrents from surface fermi arcs in topological chiral semimetals. *Phys. Rev. Lett.*, 124:166404, Apr 2020.

[7] Wanxiang Feng, Jun Wen, Jinjian Zhou, Di Xiao, and Yugui Yao. First-principles calculation of z2 topological invariants within the fp-lapw formalism. *Computer Physics Communications*, 183(9):1849–1859, 2012.

[8] Liang Fu and C. L. Kane. Topological insulators with inversion symmetry. *Phys. Rev. B*, 76:045302, Jul 2007.

[9] Liang Fu, C. L. Kane, and E. J. Mele. Topological insulators in three dimensions. *Phys. Rev. Lett.*, 98:106803,

Mar 2007.

[10] Takahiro Fukui and Yasuhiro Hatsugai. Quantum spin hall effect in three dimensional materials: Lattice computation of z2 topological invariants and its application to bi and sb. *Journal of the Physical Society of Japan*, 76(5):053702, 2007.

[11] Zihao Gao, Meng Hua, Haijun Zhang, and Xiao Zhang. Classification of stable dirac and weyl semimetals with reflection and rotational symmetry. *Phys. Rev. B*, 93:205109, May 2016.

[12] Ce Huang, Benjamin T. Zhou, Huiqin Zhang, Bingjia Yang, Ran Liu, Hanwen Wang, Yimin Wan, Ke Huang, Zhiming Liao, Enze Zhang, Shanshan Liu, Qingsong Deng, Yanhui Chen, Xiaodong Han, Jin Zou, Xi Lin, Zheng Han, Yihua Wang, Kam Tuen Law, and Faxian Xiu. Proximity-induced surface superconductivity in dirac semimetal cd3as2. *Nature Communications*, 10(1):2217, May 2019.

[13] Vsevolod Ivanov and Sergey Y. Savrasov. Monopole mining method for high-throughput screening for weyl semimetals. *Phys. Rev. B*, 99:125124, Mar 2019.

[14] G. S. Jenkins, C. Lane, B. Barbiellini, A. B. Sushkov, R. L. Carey, Fengguang Liu, J. W. Krizan, S. K. Kushwaha, Q. Gibson, Tay-Rong Chang, Horng-Tay Jeng, Hsin Lin, R. J. Cava, A. Bansil, and H. D. Drew. Three-dimensional dirac cone carrier dynamics in na_3Bi and cd_3as_2. *Phys. Rev. B*, 94:085121, Aug 2016.

[15] Mehdi Kargarian, Mohit Randeria, and Yuan-Ming Lu. Are the surface fermi arcs in dirac semimetals topologically protected? *Proceedings of the National Academy of Sciences*, 113(31):8648–8652, 2016.

[16] Shingo Kobayashi and Masatoshi Sato. Topological superconductivity in dirac semimetals. *Phys. Rev. Lett.*, 115:187001, Oct 2015.

[17] Congcong Le, Xianxin Wu, Shengshan Qin, Yinxiang Li, Ronny Thomale, Fu-Chun Zhang, and Jiangping Hu. Dirac semimetal in ¡i¿β¡/i¿-cui without surface fermi arcs. *Proceedings of the National Academy of Sciences*, 115(33):8311–8315, 2018.

[18] Cai-Zhen Li, Chuan Li, Li-Xian Wang, Shuo Wang, Zhi-Min Liao, Alexander Brinkman, and Da-Peng Yu. Bulk and surface states carried supercurrent in ballistic nb-dirac semimetal cd_3as_2 nanowire-nb junctions. *Phys. Rev. B*, 97:115446, Mar 2018.

[19] Tian Liang, Quinn Gibson, Mazhar N. Ali, Minhao Liu, R. J. Cava, and N. P. Ong. Ultrahigh mobility and giant magnetoresistance in the dirac semimetal cd3as2. *Nature Materials*, 14(3):280–284, Mar 2015.

[20] Ben-Chuan Lin, Shuo Wang, An-Qi Wang, Ying Li, Rong-Rong Li, Ke Xia, Dapeng Yu, and Zhi-Min Liao. Electric control of fermi arc spin transport in individual topological semimetal nanowires. *Phys. Rev. Lett.*, 124:116802, Mar 2020.

[21] Yu Miyazaki, Tomoyuki Yokouchi, Kiyou Shibata, Yao Chen, Hiroki Arisawa, Teruyasu Mizoguchi, Eiji Saitoh, and Yuki Shiomi. Quantum oscillations from fermi arc surface states in cd_3as_2 submicron wires. *Phys. Rev. Res.*, 4:L022002, Apr 2022.

[22] Philip J. W. Moll, Nityan L. Nair, Toni Helm, Andrew C. Potter, Itamar Kimchi, Ashvin Vishwanath, and James G. Analytis. Transport evidence for fermi-arc-mediated chirality transfer in the dirac semimetal cd3as2. *Nature*, 535(7611):266–270, Jul 2016.

[23] Adriano Mosca Conte, Olivia Pulci, and Friedhelm Bechstedt. Electronic and optical properties of topological semimetal cd3as2. *Scientific Reports*, 7(1):45500, Apr 2017.

[24] Yusuke Nakazawa, Masaki Uchida, Shinichi Nishihaya, Markus Kriener, Yusuke Kozuka, Yasujiro Taguchi, and Masashi Kawasaki. Structural characterisation of high-mobility cd3as2 films crystallised on srtio3. *Scientific Reports*, 8(1):2244, Feb 2018.

[25] D. Neubauer, J. P. Carbotte, A. A. Nateprov, A. Löhle, M. Dressel, and A. V. Pronin. Interband optical conductivity of the [001]-oriented dirac semimetal cd_3as_2. *Phys. Rev. B*, 93:121202, Mar 2016.

[26] Madhab Neupane, Su-Yang Xu, Raman Sankar, Nasser Alidoust, Guang Bian, Chang Liu, Ilya Belopolski, Tay-Rong Chang, Horng-Tay Jeng, Hsin Lin, Arun Bansil, Fangcheng Chou, and M. Zahid Hasan. Observation of a three-dimensional topological dirac semimetal phase in high-mobility cd3as2. *Nature Communications*, 5(1):3786, May 2014.

[27] Hui Pan, Meimei Wu, Ying Liu, and Shengyuan A. Yang. Electric control of topological phase transitions in dirac semimetal thin films. *Scientific Reports*, 5(1):14639, Sep 2015.

[28] Mikhail Patrashin, Norihiko Sekine, Kouichi Akahane, Akifumi Kasamatsu, and Iwao Hosako. Dirac semimetal states in engineered zero-gap inas/gainsb superlattices. *physica status solidi (b)*, 256(6):1800726, 2019.

[29] A. Pietraszko and K. Łukaszewicz. A refinement of the crystal structure of α"-Cd_3As_2. *Acta Crystallographica Section B*, 25(5):988–990, May 1969.

[30] A. Rancati, N. Pournaghavi, M. F. Islam, A. Debernardi, and C. M. Canali. Impurity-induced topological phase transitions in cd_3as_2 and na_3Bi dirac semimetals. *Phys. Rev. B*, 102:195110, Nov 2020.

[31] Giacomo Resta, Shu-Ting Pi, Xiangang Wan, and Sergey Y. Savrasov. High surface conductivity of fermi-arc electrons in weyl semimetals. *Phys. Rev. B*, 97:085142, Feb 2018.

[32] Antonio Rossi, Vsevolod Ivanov, Sudheer Sreedhar, Adam L. Gross, Zihao Shen, Eli Rotenberg, Aaron Bostwick, Chris Jozwiak, Valentin Taufour, Sergey Y. Savrasov, and Inna M. Vishik. Electronic structure and topology across T_c in the magnetic weyl semimetal $co_3sn_2s_2$. *Phys. Rev. B*, 104:155115, Oct 2021.

[33] S. Roth, H. Lee, A. Sterzi, M. Zacchigna, A. Politano, R. Sankar, F. C. Chou, G. Di Santo, L. Petaccia, O. V. Yazyev, and A. Crepaldi. Reinvestigating the surface and bulk electronic properties of cd_3as_2. *Phys. Rev. B*, 97:165439, Apr 2018.

[34] S. Y. Savrasov. Linear-response calculations of lattice dynamics using muffin-tin basis sets. *Phys. Rev. Lett.*, 69:2819, 1992.

[35] S. Y. Savrasov, D. Y. Savrasov, and O. K. Andersen. Linear-response calculations of electron-phonon interactions. *Phys. Rev. Lett.*, 72:372–375, Jan 1994.

[36] Omor F. Shoron, Timo Schumann, Manik Goyal, David A. Kealhofer, and Susanne Stemmer. Field-effect transistors with the three-dimensional Dirac semimetal cadmium arsenide. *Applied Physics Letters*, 115(6):062101, 08 2019.

[37] O. O. Shvetsov, V. D. Esin, A. V. Timonina, N. N. Kolesnikov, and E. V. Deviatov. Surface superconductivity in a three-dimensional cd_3as_2 semimetal at the interface with a gold contact. *Phys. Rev. B*, 99:125305,

Mar 2019.

[38] G. A. Steigmann and J. Goodyear. The crystal structure of Cd_3As_2. *Acta Crystallographica Section B*, 24(8):1062–1067, Aug 1968.

[39] Shunxi Tang, Wang Chen, Qian Ye, Zhengfang Liu, Qingping Wu, Yan Du, Xiaoying Zhou, and Xianbo Xiao. Electron transport probing the electrically tunable topological phase transition in a dirac semimetal. *Phys. Rev. B*, 104:205427, Nov 2021.

[40] M. v. Stackelberg and R. Paulu. Untersuchungen an den phosphiden und arseniden des zinks und cadmiums. das zn3p2-gitter. *Zeitschrift für Physikalische Chemie*, 28B(1):427–460, 1935.

[41] Xiangang Wan, Ari M. Turner, Ashvin Vishwanath, and Sergey Y. Savrasov. Topological semimetal and fermi-arc surface states in the electronic structure of pyrochlore iridates. *Phys. Rev. B*, 83:205101, May 2011.

[42] Bob Minyu Wang, Yuqing Zhu, Henry Clark Travaglini, Sergey Y. Savrasov, and Dong Yu. Schottky electric field induced circular photogalvanic effect in cd3as2 nanobelts, 2022.

[43] He Wang, Huichao Wang, Haiwen Liu, Hong Lu, Wuhao Yang, Shuang Jia, Xiong-Jun Liu, X. C. Xie, Jian Wei, and Jian Wang. Observation of superconductivity induced by a point contact on 3d dirac semimetal cd3as2 crystals. *Nature Materials*, 15(1):38–42, Jan 2016.

[44] Zhijun Wang, Hongming Weng, Quansheng Wu, Xi Dai, and Zhong Fang. Three-dimensional dirac semimetal and quantum transport in cd_3as_2. *Phys. Rev. B*, 88:125427, Sep 2013.

[45] Cai-Zhi Xu, Yang-Hao Chan, Yige Chen, Peng Chen, Xiaoxiong Wang, Catherine Dejoie, Man-Hong Wong, Joseph Andrew Hlevyack, Hyejin Ryu, Hae-Young Kee, Nobumichi Tamura, Mei-Yin Chou, Zahid Hussain, Sung-Kwan Mo, and Tai-Chang Chiang. Elemental topological dirac semimetal: α-sn on insb(111). *Phys. Rev. Lett.*, 118:146402, Apr 2017.

[46] Qiunan Xu, Enke Liu, Wujun Shi, Lukas Muechler, Jacob Gayles, Claudia Felser, and Yan Sun. Topological surface fermi arcs in the magnetic weyl semimetal co3sn2s2. *Phys. Rev. B*, 97:235416, Jun 2018.

[47] Binghai Yan and Claudia Felser. Topological materials: Weyl semimetals. *Annual Review of Condensed Matter Physics*, 8(1):337–354, 2017.

[48] Hemian Yi, Zhijun Wang, Chaoyu Chen, Youguo Shi, Ya Feng, Aiji Liang, Zhuojin Xie, Shaolong He, Junfeng He, Yingying Peng, Xu Liu, Yan Liu, Lin Zhao, Guodong Liu, Xiaoli Dong, Jun Zhang, M. Nakatake, M. Arita, K. Shimada, H. Namatame, M. Taniguchi, Zuyan Xu, Chuangtian Chen, Xi Dai, Zhong Fang, and X. J. Zhou. Evidence of topological surface state in three-dimensional dirac semimetal cd3as2. *Scientific Reports*, 4(1):6106, Aug 2014.

[49] Cheng Zhang, Awadhesh Narayan, Shiheng Lu, Jinglei Zhang, Huiqin Zhang, Zhuoliang Ni, Xiang Yuan, Yanwen Liu, Ju-Hyun Park, Enze Zhang, Weiyi Wang, Shanshan Liu, Long Cheng, Li Pi, Zhigao Sheng, Stefano Sanvito, and Faxian Xiu. Evolution of weyl orbit and quantum hall effect in dirac semimetal cd3as2. *Nature Communications*, 8(1):1272, Nov 2017.

[50] Cheng Zhang, Zhuoliang Ni, Jinglei Zhang, Xiang Yuan, Yanwen Liu, Yichao Zou, Zhiming Liao, Yongping Du, Awadhesh Narayan, Hongming Zhang, Tiancheng Gu, Xuesong Zhu, Li Pi, Stefano Sanvito, Xiaodong Han, Jin Zou, Yi Shi, Xiangang Wan, Sergey Y. Savrasov, and Faxian Xiu. Ultrahigh conductivity in weyl semimetal nbas nanobelts. *Nature Materials*, 18(5):482–488, May 2019.

[51] Dong Zhang, Wenkai Lou, Maosheng Miao, Shou-cheng Zhang, and Kai Chang. Interface-induced topological insulator transition in GaAs/Ge/GaAs quantum wells. *Phys. Rev. Lett.*, 111:156402, Oct 2013.

[52] Yanfei Zhao, Haiwen Liu, Chenglong Zhang, Huichao Wang, Junfeng Wang, Ziquan Lin, Ying Xing, Hong Lu, Jun Liu, Yong Wang, Scott M. Brombosz, Zhili Xiao, Shuang Jia, X. C. Xie, and Jian Wang. Anisotropic fermi surface and quantum limit transport in high mobility three-dimensional dirac semimetal cd_3as_2. *Phys. Rev. X*, 5:031037, Sep 2015.

[53] Guolin Zheng, Min Wu, Hongwei Zhang, Weiwei Chu, Wenshuai Gao, Jianwei Lu, Yuyan Han, Jiyong Yang, Haifeng Du, Wei Ning, Yuheng Zhang, and Mingliang Tian. Recognition of fermi-arc states through the magnetoresistance quantum oscillations in dirac semimetal Cd_3As_2 nanoplates. *Phys. Rev. B*, 96:121407, Sep 2017.